Taylor & Francis
Taylor & Francis Group

H.L. ROY MEMORIAL LECTURE SPONSORED BY JACOBS H & G
A Smörgåsbord of Separation Strategies Using Microporous Crystalline Materials[†]

Rajamani Krishna[*]
Van't Hoff Institute for Molecular Sciences, University of Amsterdam, Amsterdam, The Netherlands

Abstract: Ordered crystalline microporous materials such as zeolites, metal-organic frameworks and zeolitic imidazolate frameworks, with pores in the 3–20 Å range, offer considerable potential for use in a wide variety of separations in the process industries. For many separation tasks, microporous adsorbents and membranes are energy-efficient alternatives, or adjuncts, to conventional distillation technology. Molecular insights and molecular simulation techniques allow us to identify the microporous material with the ideal pore size that offers the right degree of interactions (such as van der Waals, electrostatic, π-electron exchange) with the guest molecules to achieve the best separation. Particularly noteworthy are possibilities of separations on the basis of subtle differences in molecular configurations, and the efficiencies with which molecules pack or stack within the microporous channels.

Keywords: Binding energy, Diffusion selectivity, Molecular configurations, Packing efficiencies, Isomer separations

Introduction

Separation technologies such as distillation, absorption and extraction are energy-intensive because of vapour/liquid phase transformations in condensers, reboilers and solvent recovery sections. The energy consumption for distillation accounts for about 50% of the total energy consumption for all separations [1]. The largest opportunities for energy reduction are offered

---

*Author for Correspondence. Email: r.krishna@uva.nl
[†]This lecture was delivered at CHEMCON 2013, held in Mumbai, India during 27–30 December 2013.

by replacing distillation with (a) low-energy-demanding separation systems such as adsorption or membranes, or (b) hybrid systems that combine distillation with adsorption or membranes [1]. In many cases, the hybrid processing option is easier to implement technically because adsorption and membrane separations often cannot produce products with the purity levels that are achievable with distillation. The success of such replacement strategies is crucially dependent on development of suitable porous materials that can be used in fixed bed adsorption devices or as thin layers in membrane permeation units.

The most commonly understood separation principles using porous materials involve distinguishing molecules on the basis of (a) size and mobility, (b) van der Waals interactions and polarizability, (c) electrostatic interactions and (d) π-electron transfers. Additional separation strategies become possible by use of ordered crystalline materials with channel dimensions in the 3–20 Å range, that is, of the same order of magnitude as the guest molecules.

During the last two decades, there has been considerable research effort on the synthesis of ordered crystalline microporous materials such as metal–organic frameworks (MOFs), covalent–organic frameworks and zeolitic imidazolate frameworks (ZIFs) [2–5]; these materials have potential applications in a variety of separations [6–8]. MOFs are a class of crystalline organic–inorganic hybrid compounds formed by coordination of metal ions (e.g. Zn, Cu, Cr, Al, Zr, Mg, Ni, Fe), or clusters, with organic linkers (bivalent or trivalent aromatic carboxylic acids or azoles) to form robust porous periodic frameworks. For example, Zn_4O groups are linked with terephthalate (= 1,4 benzenedicarboxylate (BDC)) to form $Zn_4O(BDC)_3$, commonly known as MOF-5 or IRMOF-1. Particularly potent for separations are MOFs with coordinatively unsaturated metal centres that may be created by evacuation of frameworks that have metal-bound solvent molecules. This strategy has been employed to expose M^{2+} cation sites in some of the most widely studied frameworks, such as $M_2(dobdc)$ (M = Mg, Mn, Co, Ni, Zn, Fe; $dobdc^{4-}$ = 2,5-dioxido-1,4-benzenedicarboxylate; these MOFs are also referred to as MMOF-74 and CPO-27-M; see framework in Fig. 1) and $M_3(BTC)_2$ (M = Cu, Cr, Mo; BTC^{3-} = 1,3,5-benzenetricarboxylate; $Cu_3(BTC)_2$ is also known as HKUST-1).
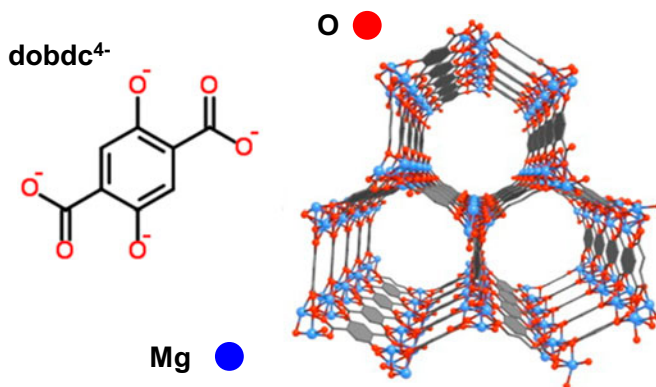

Fig. 1. MgMOF-74 has 1D hexagonal-shaped channels of 11 Å size.

In ZIFs, the Zn or Co atoms are linked through N atoms of ditopic imidazolates to form a range of neutral framework structures. The frameworks of ZIF compounds can be represented by M(Im)$_2$ (M = tetrahedrally coordinated metal atom; Im = imidazolate and its derivative), similar to that of $(AlO_2)_x(SiO_2)_y$ zeolites. The M–Im–M angle of 145° is close to the Si–O–Si angle typically found in zeolites. ZIF-8, for example, has the structural topology of SOD (sodalite), and consists of cages separated by narrow windows.

In comparison to traditionally used porous materials such as zeolites, MOFs and ZIFs offer significantly higher surface areas and porosities (Fig. 2) [9–11]. The commonly used MFI zeolite, for example, has a characteristic channel dimension of 5.5 Å, a pore volume of 0.165 cm^3/g, and a surface area of 490 m^2/g. The accessible pore volumes of MOFs are commonly in the 0.5–2 cm^3/g range. Significantly higher surface areas are available with MOFs; for example MOF-177 has an area of 4800 m^2/g. The pore dimensions of MOFs cover a much wider range: ZIF-8 has a window aperture of 3.3 Å, and MgMOF-74 has one-dimensional (1D) hexagonal shaped channels of 11 Å.

Framework flexibility has, in most cases, a negligible influence on the adsorption and diffusion characteristics of zeolites [12]; this is because zeolite frameworks are constructed with strong covalent bonds that are rigid [13]. On the other hand, many MOFs and ZIFs possess soft "dynamic" frameworks whose cell dimensions change in a reversible manner to external stimuli. For example, IRMOF-1 exhibits negative thermal expansion [14]. Flexible microporous chromium or iron terephtalates, MIL-53(Cr, Fe) exhibit "breathing effects" [15]. MIL-53(Cr) has a unit cell volume of 1486 Å^3 in the as-synthesized "large pore" form (-lp) (see Fig. 3a). At a water loading of two molecules per unit cell, the unit cell volume shrinks to 1013 Å^3, the "narrow pore" (-np) form (Fig. 3b) [15, 16]. The -np structure is virtually inaccessible to guest molecules. On heating and removal of adsorbed water, the -lp form is regained. The exploitation of structural changes in MIL-53 has been suggested for purpose of controlled delivery of ibuprofen [17].
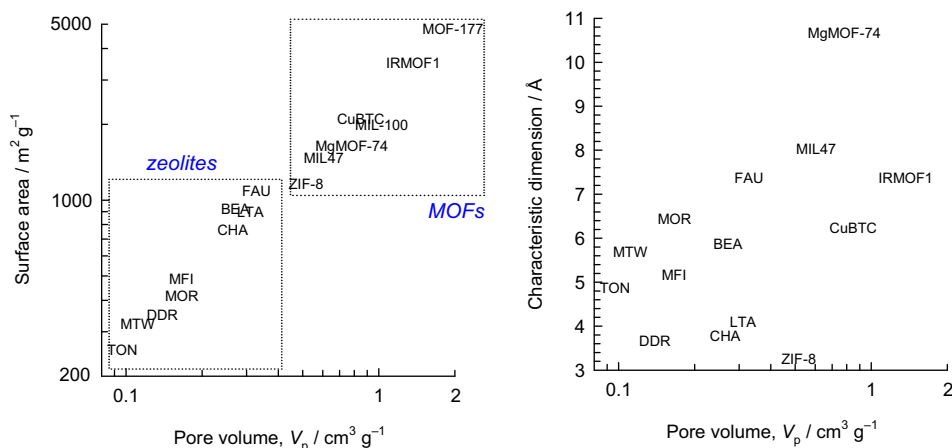

Fig. 2. Comparison of surface area, pore volumes, and characteristic dimensions of some representative zeolites, MOFs and ZIFs.

(a) MIL-53(Cr)-lp

(b) MIL-53(Cr)-np

pristine framework

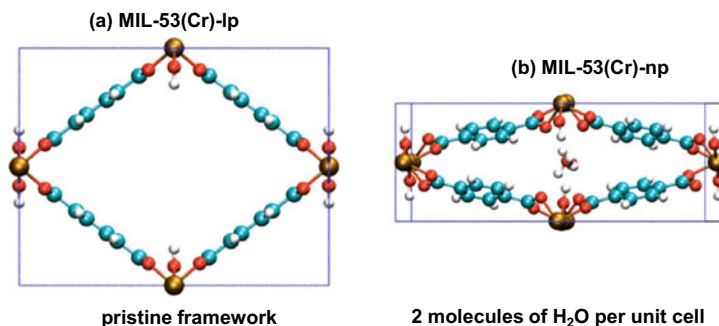**2 molecules of H$_2$O per unit cell**

Fig. 3. The framework structure MIL-53(Cr): (a) as-synthesized pristine framework, with no adsorbed water molecules; and (b) two water molecules adsorbed per unit cell.

For any given separation application, it is possible to identify the microporous material with the ideal pore size, and the surface area that offers the right degree of interactions (van der Waals, electrostatic, π-electron exchange) with the guest molecules. Additionally, we shall demonstrate that microporous crystalline materials are capable of separating molecules relying on differences in molecular configurations, molecular packing and molecular stacking within channels. The identification of the "ideal" selective adsorbent can be achieved using state-of-the-art molecular simulations of adsorption and diffusion [6, 7, 18, 19]. This allows for the possibility of bespoke tailoring of MOFs or ZIFs to meet with the separation requirement in either a fixed bed adsorber or membrane configurations.

Exploiting Differences in Binding Energies

The most common principle of separation is to exploit the differences with which the individual components in the mixture adsorb, that is, "bind", with the framework. For CO_2 capture from flue gas, and natural gas, we can rely on selective CO_2 binding with extra-framework cations (e.g. Na$^+$, K$^+$, Ca^{2+}, Ba^{2+}) of zeolites 13X, 3A, 4A, and 5A. With MOFs, selective CO_2 binding could, for example, be achieved with M^{2+} of M$_2$(dobdc) (Mg, Mn, Co, Ni, Zn, Fe Cu, Mg) or M^{2+} of M$_3$(BTC)$_2$ (M = Cu, Cr, Mo). Wu et al. have established that the O atoms of CO_2 bind with the Mg atoms of MgMOF-74; see Fig. 4(a). Such binding results in selective separations that can compete economically with amine absorption [20–29]. The stronger the binding, the higher the selectivity is for separations. The binding of CO_2 with Mg^{2+} atoms of MgMOF-74 has an associated binding energy of 42 kJ/mol, and the obtained CO_2/N_2, CO_2/CH_4 and CO_2/H_2 selectivities are higher than for other materials such as 13X, LTA-5A, and Cu$_3$(BTC)$_2$ [20, 21, 23–25, 30]. However, stronger binding leads to higher regeneration costs in pressure swing adsorption (PSA) or temperature swing adsorption (TSA) operations. The choice of the adsorbent material must strike the right balance between adsorption selectivity, uptake capacity and binding energy [8, 21]. Duan et al. [29] have suggested the use of PCP-1 (= La(BTN)) for CO_2 capture from typical flue gas mixtures containing 15% CO_2, 1% CO, 4% O_2, and 80% N_2 on the basis of its low binding energy, about 28 kJ/mol.
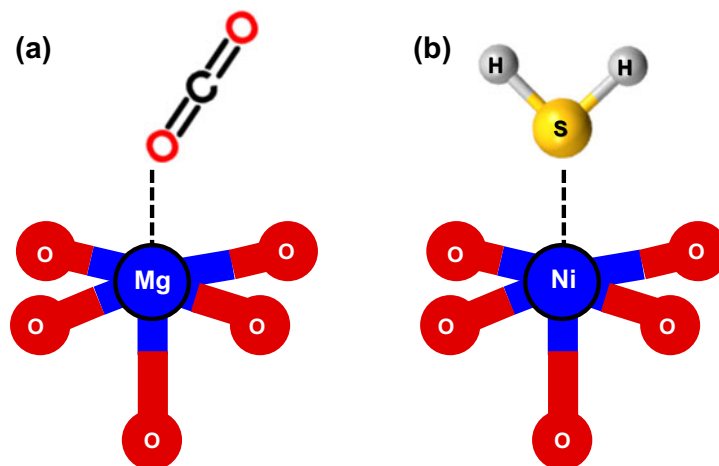
Fig. 4. (a) O atom of CO_2 binds with metal atoms of MgMOF-74 [90]. (b) S atoms of H_2S bind with metal atoms of NiMOF-74 [31].

The production of pure H_2 from steam–methane reformer off-gas requires the operation of PSA units at pressures reaching about 5 MPa. MOFs with "open" structures, that is, with large pore volumes, such as Cu-TDPAT and $Cu_3(BTC)_2$, are attractive because they have high adsorption capacities, and the binding energy has an acceptable value [8, 21]. Figure 5 shows the transient breakthrough characteristics of an adsorber packed with Cu-TDPAT [8]. The sequence of breakthroughs is H_2, N_2, CH_4, CO and CO_2. H_2, of the required 99.95% purity, can be recovered in the early stages of the transience.

The binding of H_2S with metal atoms of MOFs is much stronger than that with CO_2, and this is reflected in a higher heat of adsorption [31]. In this case, the binding is between the S
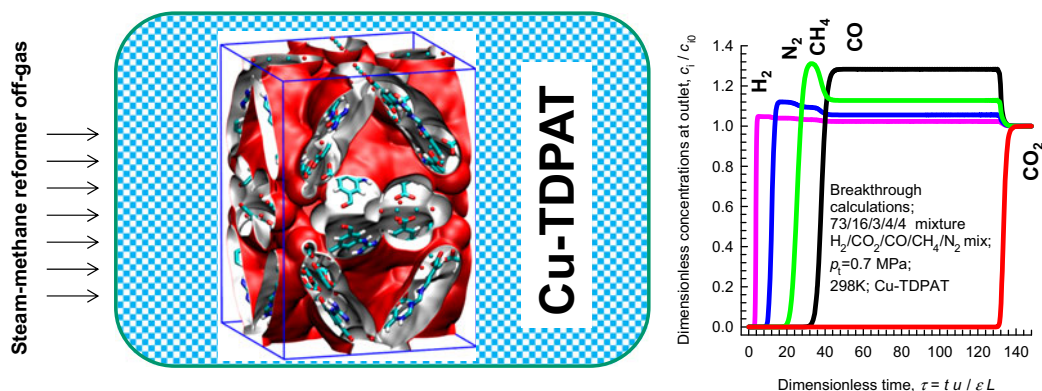

Fig. 5. Breakthrough characteristics of 5-component 73/16/3/4/4 $H_2/CO_2/CO/CH_4/N_2$ mixture in adsorber packed with Cu-TDPAT.
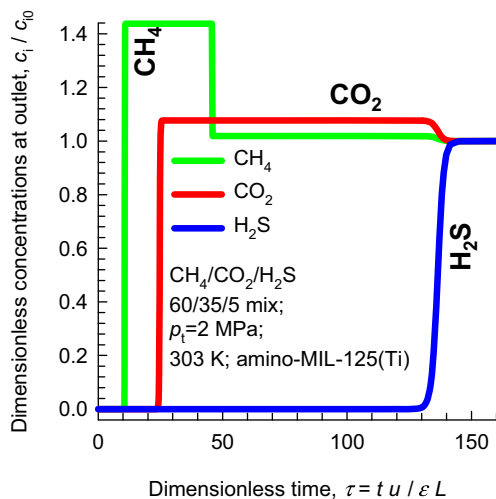
Fig. 6. Simulation of transient breakthroughs in fixed bed adsorber with input of 35/60/5 CO_2/CH_4/H_2S mixture using amino-MIL-125(Ti).

atoms with NiMOF-74; see Fig. 4(b). Vaesen et al. [32] present adsorption isotherm data to demonstrate the potential of amino-MIL-125(Ti) for the removal of both CO_2 and H_2S from natural gas. Simulation of transient breakthroughs in a fixed bed adsorber with step input of 35:60:5 CO_2/CH_4/H_2S mixtures operating at 2 MPa is shown in Fig. 6 [8]. The breakthrough of H_2S occurs much later than that of CO_2. The isosteric heat of adsorption of CO_2 in amino-MIL-125(Ti) is 30 kJ/mol, significantly lower than materials such as MgMOF-74, Cu-TDPAT and NaX zeolite; this is a desirable feature as it implies lower regeneration energy requirements.

Using breakthrough experiments, Britt et al. [33] compared the efficacy of a variety of MOFs for the removal of eight harmful gases (CO, SO_2, NH_3, Cl_2, CH_2Cl_2, C_2H_4O, benzene and tetrahydrothiophene) and found $Cu_3(BTC)_2$ to match or outperform the commonly used BPL activated carbon.

The separation of C_2H_2/C_2H_4 can be achieved using FeMOF-74 (see Fig. 7) because C_2H_2 binds more strongly than C_2H_4 [34, 35]. The high C_2H_2 adsorption selectivity with FeMOF-74 is due to the side-on π-coordination of C_2H_2 with the Fe^{2+} [35, 36]. The use of FeMOF-74 in PSA units could supplant the commonly used DMF absorption technology.

Materials such as MgMOF-74, CoMOF-74 and FeMOF-74 are not only capable of separating C_2H_2/C_2H_4 mixtures but can also fractionate a mixture containing C1, C2 and C3 hydrocarbons to recover each individual component into its relatively pure form [8, 34, 35]. This is illustrated in Fig. 8(a) by pulse chromatographic separation of a six-component CH_4/C_2H_2/C_2H_4/C_2H_6/C_3H_6/C_3H_8 mixture with MgMOF-74. The sequence of breakthroughs – CH_4, C_2H_6, C_3H_8, C_2H_4, C_2H_2 and C_3H_6 – is dictated by a combination of chain length and degree of unsaturation, and is essentially a reflection of the hierarchy of binding energies.
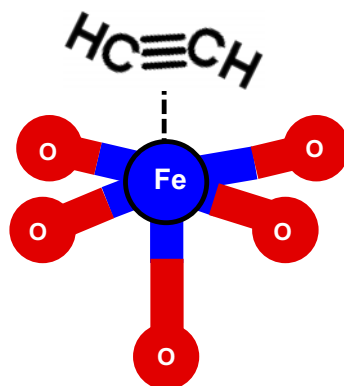
Fig. 7. C_2H_2 binds with Fe atoms of FeMOF-74.

MgMOF-74, CoMOF-74, and FeMOF-74 have potential for use in the separation train for natural gas liquids. While fractionation into individual components is desirable in some cases, M-MOF-74 suffers from the important disadvantage that the binding energies of the unsaturated C_2H_4, C_2H_2 and C_3H_6 are very high, and this results in high regeneration costs. Owing to their stronger binding, the unsaturated alkenes elute later than the corresponding saturated alkanes. MgMOF-74, CoMOF-74 and FeMOF-74 have been suggested as being suitable for C_2H_4/C_2H_6, and C_3H_6/C_3H_8 separations that are important for the production of 99.95% pure polymer-grade feedstocks. However, the desired pure alkenes can only be
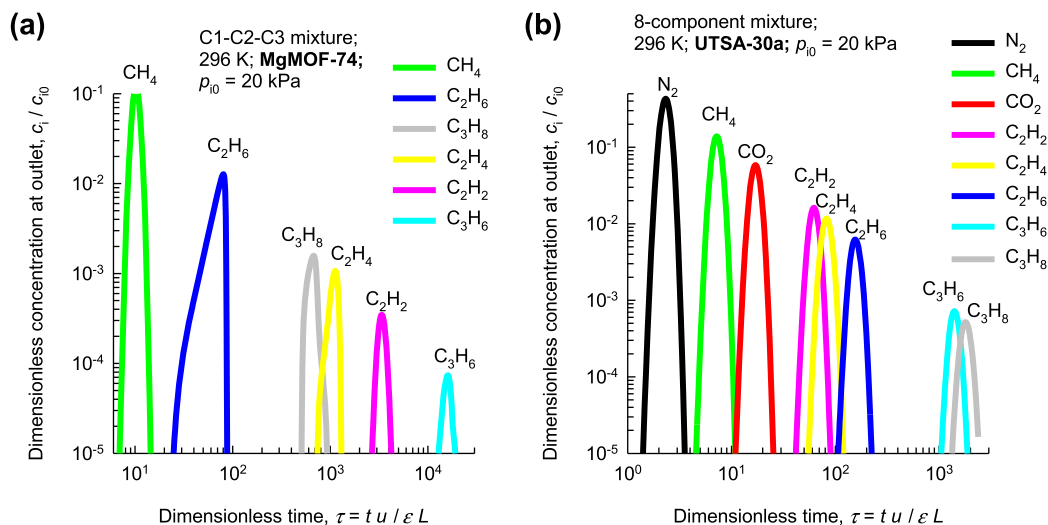

Fig. 8. (a) Fractionation of mixture of C1, C2 and C3 hydrocarbons into individual components using MgMOF-74. (b) Fractionation of mixture of C1, C2 and C3 hydrocarbons, along with N_2 and CO_2 using UTSA-30a.

recovered in the desorption cycle; this is undesirable from a practical view point. It is preferable to use adsorbents that are selective to the saturated alkanes, so that the desired alkenes are recoverable in the adsorption cycle [37]. The preferential adsorption of alkanes is only possible if separations are based on van der Waals interactions alone. This scenario holds in all-silica zeolites [38], ZIF-7 [37] and ZIF-8 [39]. However, the adsorption selectivities cannot be expected to be high. Indeed, computational screening of 300,000 all-silica structures by Kim et al. [38] resulted in the "discovery" of SOF, which has a C_2H_6/C_2H_4 selectivity of only 2.9.

Another option for separation of a mixture of C1, C2 and C3 hydrocarbons, also containing N_2 and CO_2, is to use the Yb-MOF (UTSA-30a). The breakthrough simulations of He et al. [40] show that the mixture can be separated into five fractions: N_2, CH_4, CO_2, C2 and C3 (see Fig. 8b). The significantly lower binding energy in Yb-MOF is an important advantage over M-MOF-74. The ability of UTSA-30a to separate CO_2 from C_2H_6 is of practical importance because current technology uses extractive distillation for this separation [41].

The removal and recovery of xenon (Xe) and krypton (Kr) from process off-gases from nuclear plants, typically present in concentrations of 400 and 40 ppm, respectively, is an important problem [42]. Liu et al. [42] have presented isotherm and breakthrough data to demonstrate the efficacy of Ni_2(dobdc) (= NiMOF-74 = CPO-27-Ni) for use in this separation task. It is possible to recover both Xe and Kr in nearly pure forms using this material [8].

There are several examples where it is required to separate mixtures of aromatics and aliphatic compounds [8]. Cyclohexane, an important industrial chemical, is produced by catalytic hydrogenation of benzene. The unreacted benzene is present in the effluent from the reactor must be removed from the desired product. The separation of benzene and cyclohexane is difficult because the differences in the boiling points is only 0.6 K. Currently technologies use extractive distillation with entrainers such as sulpholane, dimethylsulfoxide, N-methylpyrrolidone and N-formylmorpholine; such processes are energy intensive. Adsorptive separations offer the energy-efficient alternatives to extractive distillation, especially for mixtures containing a small percentage of benzene, as is commonly encountered.

Takahashi and Yang [43] have presented pure component isotherm data for benzene and cyclohexane to show that cation-exchanged Na–Y, Pd–Y and Ag–Y zeolites (all with FAU topology) have high selectivity for adsorption of benzene, owing to π-complexation; cyclohexane does not form π-complexes.

An alternative suggested by Ren et al. [44] is to use a porous aromatic framework, PAF-2. The pure component isotherm data for PAF-2 shows excellent selective sorption of benzene. The much higher uptake of benzene compared with cyclohexane is due to the π–π interaction between the benzene molecule and the aromatic framework of PAF-2.

Hexane, used as solvent for oil seeds extraction, has to conform to food-grade specifications that stipulate a maximum of 1.3 wt% aromatics. The source for food-grade hexane is straight-run naphtha with a narrow 63–69°C cut; this cut usually contains more than the stipulated maximum concentration of aromatics and is as high as 14% for Bombay High crude oil [45]. In the technology currently in use in Indian refineries, food-grade hexane is produced by liquid extraction with NMP as solvent [45]. Ag–Y and NaX could perhaps be

used for selective removal of benzene from the 63–69°C naphtha cut [8]; this needs further investigation.

Exploiting Differences in Diffusivities

To get an appreciation of diffusion selective separations, let us consider the LTA zeolite for which the all-silica form (i.e. without cations, also called ZK-4) has a window size of approximately 4.1 × 4.7 Å. Figure 9 presents snapshots showing the location of cations in the industrially important LTA-4A (96 Si, 96 Al, 96 Na^+, Si/Al = 1) and LTA-5A (96 Si, 96 Al, 32 Na^+, 32 Ca^{2+}, Si/Al = 1) zeolites. In LTA-4A, some of the Na^+ cations partially block the window regions [46–50], thereby effectively reducing the aperture size that is available for inter-cage hopping of molecules. The Na^+ and Ca^{2+} cations in LTA-5A, on the other hand, do not locate near the window regions and there is no blocking. This implies that diffusional influences are much stronger in LTA-4A than in LTA-5A zeolite. The presence of bulkier K^+ cations in LTA-3A (96 Si, 96 Al, 96 K^+, Si/Al = 1) causes the window blocking effect to be significantly enhanced, when compared with LTA-4A. For this reason, LTA-3A zeolite is used for selective removal of water from gaseous streams (dehumidification) and water–alcohol (dehydration) mixtures [51]. It has to be mentioned that it is common to find information in the published literature that suggest that 3A, 4A and 5A zeolites have window apertures, respectively, of 3, 4 and 5 Å; this is not precisely correct. The degree of blocking (by the cations Na^+ or K^+) of the window apertures of the pristine framework with 4.1 × 4.7 Å decreases in the order as we progress from 3A to 4A to 5A.

The best illustration of the dramatic influence of the window aperture is to consider the separation of O_2/N_2 mixtures. Both O_2 and N_2 have similar polarizabilities and magnetic susceptibilies. However, the quadrupole moment of N_2 is about 4 times that of O_2; for both LTA-4A, and LTA-5A the adsorption selectivity is in favour of N_2. In LTA-5A zeolite the ratio of the diffusivity of O_2 to that of N_2 is 2 [8]. In a fixed bed adsorber with LTA-5A, O_2 breakthrough occurs earlier than that of N_2 because the separation is governed by
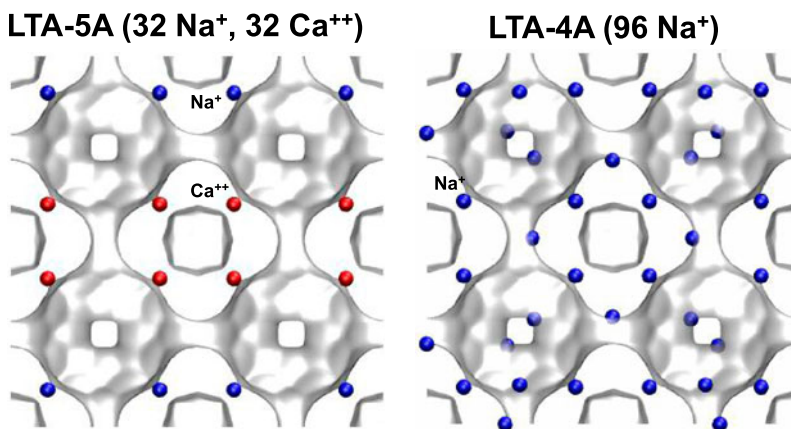

Fig. 9. Snapshots showing the location of cations in LTA-5A and LTA-4A.

thermodynamic equilibrium that overrides the diffusional effects. The general rule is that adsorption strength does not go hand-in-hand with molecular mobility or diffusivity [11, 52, 53]. Depending on the choice of the material, one of these two factors "wins" and determines the overall selectivity of separation. Purified O_2 is the product emerging from the adsorption cycle of a fixed bed packed with LTA-5A.

Owing to the reduced window aperture of LTA-4A, the ratio of the ratio of the diffusivity of O_2 to that of N_2 is about 100. A fixed bed adsorber packed with LTA-4A produces pure N_2 in the adsorption phase of PSA operations, that is, the separation is diffusion-selective. The use of carbon molecular sieves also results in diffusion-selective separation that produces purified N_2. Generally speaking, diffusion-selective separations have undesirably short cycle times in PSA units when compared with equilibrium-based separations. A better strategy is to use an adsorption selective process with selective binding of O_2 to the Fe^{2+} of FeMOF-74 because of the greater electron affinity of O_2 than N_2 (see Fig. 10); this can be exploited to separate O_2/N_2 mixtures for production of pure N_2 [8, 54].

Let us consider the separation of a 50:50 ethanol/water mixture. Distillation can produce ethanol with a purity close to 95 wt% owing to azeotrope formation. For obtaining, say, 99.5% pure ethanol, we need to feed the obtained 95 wt% ethanol product to an azeotropic distillation column with an entrainer such as benzene or cyclohexane. A better alternative, avoiding the use of entrainers, is to adopt a hybrid scheme (see Fig. 11) in which the 95 wt% ethanol top product is fed to a hydrophilic LTA-4A zeolite membrane pervaporation unit. LTA-4A zeolite has 11 Å sized cages separated by windows with an aperture of 4 Å. Water has a significantly higher diffusivity than ethanol owing to the narrow window aperture;
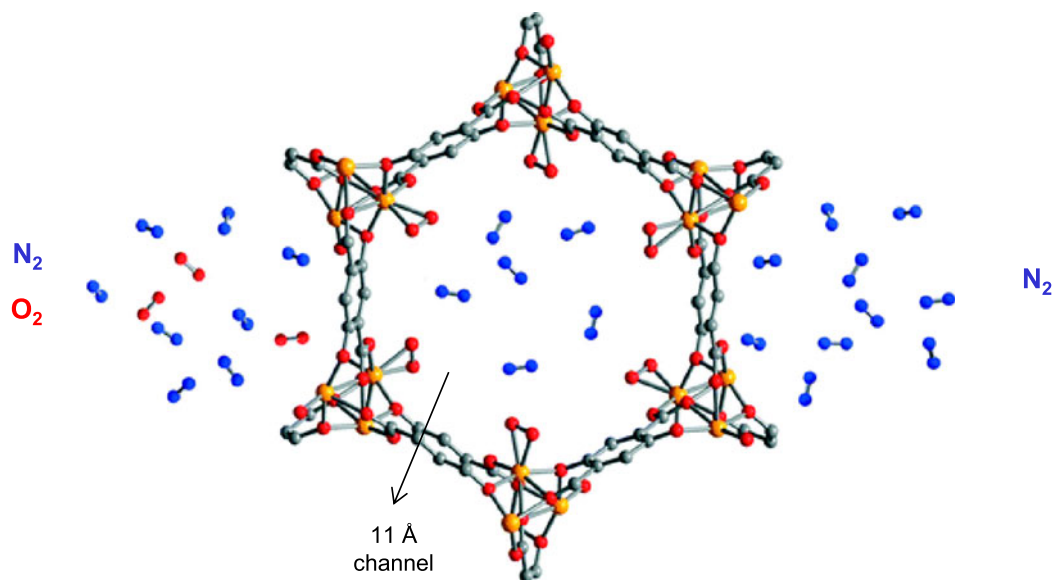

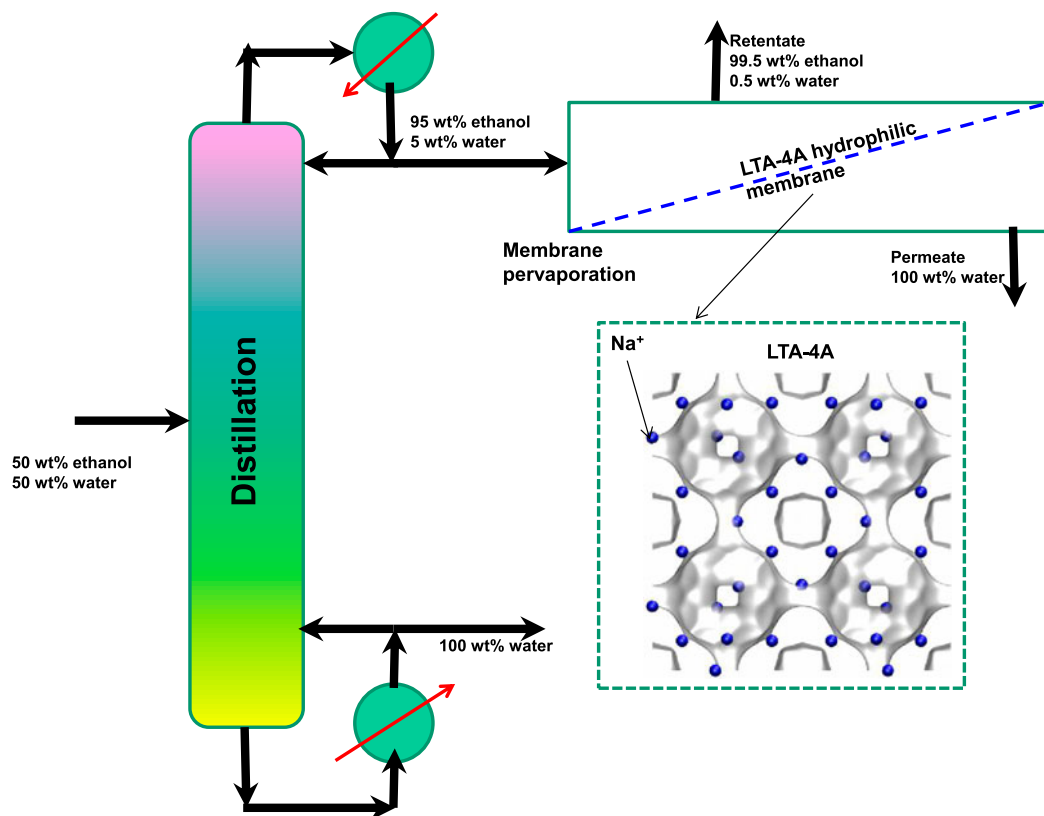**Fig. 10**. O atom of oxygen binds with Fe atoms of FeMOF-74.

Fig. 11. Water permeates preferentially across LTA-4A zeolite membrane used in hybrid scheme for production of 99.5% pure ethanol.

diffusion selectivity strongly favours water. The desired 99.5% pure ethanol product is recovered as retentate.

A different strategy, using ZIF-8 membrane, could lead to energy reductions to the scheme sketched in Fig. 11. ZIF-8 is hydrophobic and the adsorption selectivity is strongly in favour of ethanol [55]. Unlike LTA-4A, the windows of ZIF-8 are not rigid. Framework flexibility allows larger molecules to diffuse through the window aperture. The principle of separation of water and ethanol favours ethanol for two reasons: (a) much stronger adsorption of ethanol; and (b) framework flexibility allowing ethanol to hop from one cage to the next with acceptable mobility. Ethanol–water permeation across a ZIF-8 membrane produces a permeate that is richer in ethanol (see Fig. 12). The use of ZIF-8 membranes has considerable potential for use in recovery of alcohols such as ethanol and 1-butanol from biofuels [55, 56].

The separation of N_2/CH_4 mixtures is important in the context of natural gas upgrading. For transportation purposes, the pipeline specifications usually demand that the amount of
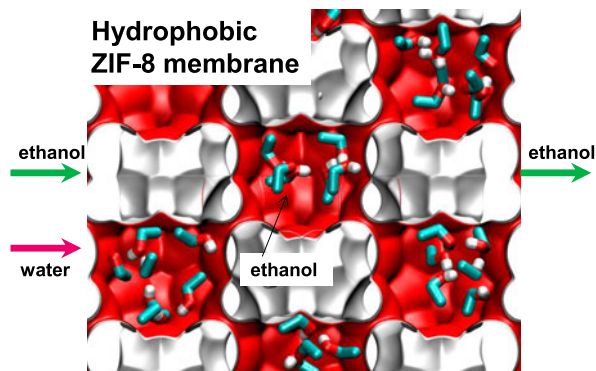
Fig. 12. Ethanol-selective permeation of ethanol/water mixture across hydrophobic ZIF-8 membrane.

N_2 in natural gas is less than about 3%, because the presence of N_2 reduces the heating value. For purification of natural gas streams, which is commonly available at high pressures, it is desirable to use adsorbents in PSA units that are selective to N_2, which is present in quantities that are often as high as 20%. For most known adsorbents, the adsorption selectivity favours CH_4. One practical solution to this problem is to rely on diffusion selectivities by using microporous materials such as LTA-4A and BaETS-4 that have significantly higher diffusivities of N_2, compared with that of CH_4 [57–59].

Ethene is an important chemical used as feedstock in manufacture of polymers such as polyethene, polyvinyl chloride, polyester and polystyrene as well as other organic chemicals. Propene is an important chemical used as feedstock in manufacture of polymers such as polypropene. Key processing steps in preparing feedstocks for polymer production are the separations of ethene/ethane, and propene/propane mixtures. The boiling points are below ambient temperatures: ethane (184.5 K), ethene (169.4 K), propane (225.4 K) and propene (225.4 K). Owing to the small differences in the boiling points, the relative volatility of ethene/ethane is 1.2; for propene/propane the relative volatility is 1.14. These separations are traditionally carried out in distillation columns that operate at high pressures and low temperatures. The purity requirement of the alkenes as feedstocks to polymerization reactors is 99.95%, and consequently the distillation columns are some of the largest and tallest columns used in the petrochemical industries with about 150–200 trays, and operating at reflux ratios of about 15.

Let us examine how a ZIF-8 membrane, used in a hybrid combination with distillation (see Fig. 13), can assist in reducing the energy consumption. The subtle differences in the bond lengths and bond angles of propene and propane cause the diffusivity of propene in ZIF-8 to be about two orders of magnitude higher than that of propane [11]. The permeation selectivity of ZIF-8 membrane is in the range of 30–35, in favour of propene [8, 60, 61]. The permeation selectivity is significantly higher than the relative volatility of 1.14; consequently the hybrid process can be expected to have superior separation capability when compared with distillation alone. Importantly, the hybrid scheme in Fig. 13 contributes to alleviating the load on the condensers and reboilers.
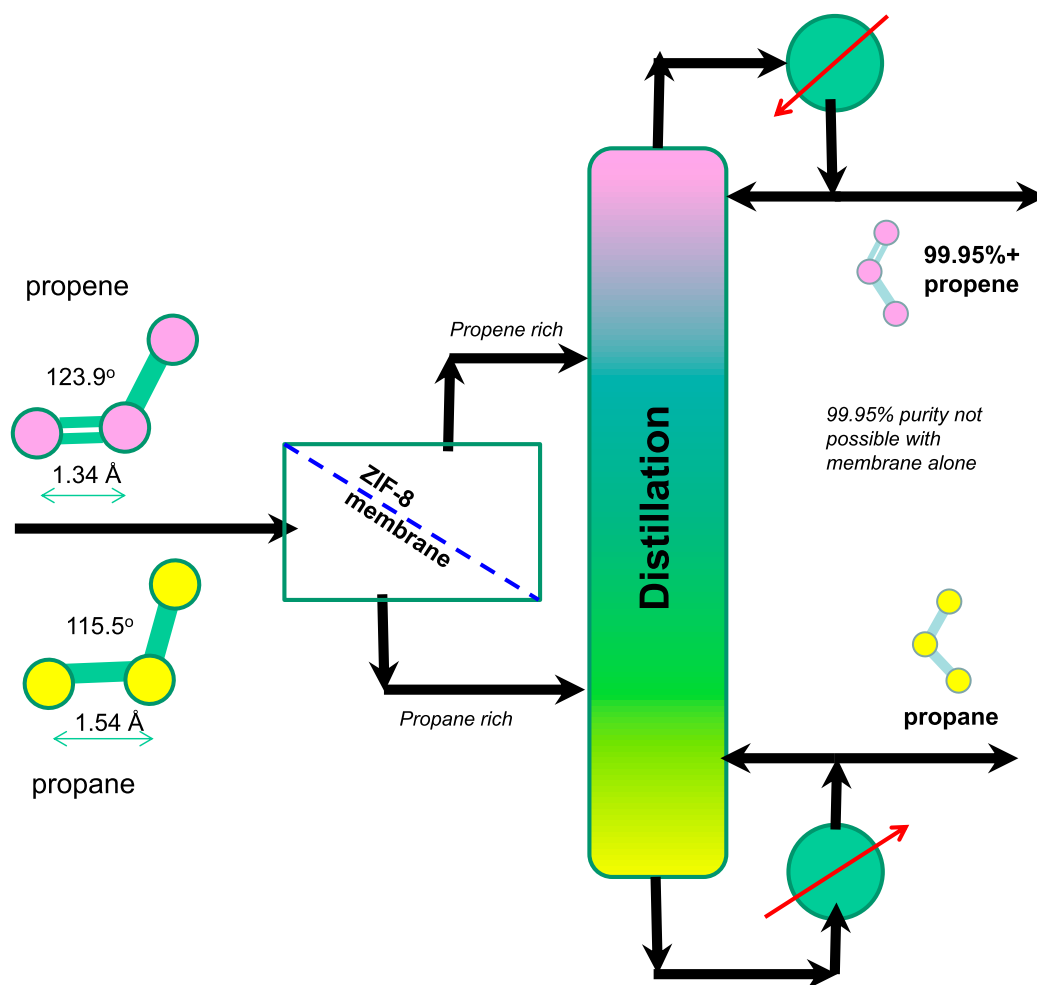
Fig. 13. Separation of propene and propane using a hybrid scheme consisting of ZIF-8 membrane and conventional distillation.

Exploiting Differences in Molecular Configurations

The separation of unsaturated alkenes from C4 hydrocarbon mixtures is important in petrochemical processing. The boiling points are *iso*-butane = 261.45K; *iso*-butene = 266.25 K; 1-butene = 266.85 K; 1,3 butadiene = 268.75 K; normal butane = 272.65 K; *trans*-2-butene = 273.45 K; and *cis*-2-butene = 276.85 K. Entrainers such as DMF, sulpholane and furfural are used in the extractive distillation of C4 fractions; solvent recovery has high associated costs. Hartmann et al. [62] have presented breakthrough experimental data to demonstrate the separation of isobutane/isobutene mixtures using $Cu_3(BTC)_2$. The adsorptive

separation step exploits the strong interactions double bond of isobutene with Cu^{2+}; the unsaturated molecules bond preferentially with the coordinatively unsatureated Cu atoms.

The separation of the *n*-butane from its isomer *iso*-butane requires exploitation of subtle configurational differences. Consider the separation of *n*-butane from *iso*-butane using MFI zeolite. The linear *n*-butane can locate anywhere along the channels (see Fig. 14a). The more compact *iso*-butane is more constrained within the 5.5 Å channels and prefers to locate at the intersections between the channels because such locations offer more "leg room" (see Fig. 14b). The number of intersection sites is restricted to a four per unit cell of MFI. To achieve loadings of *iso*-butane > 4 molecules per unit cell, an "extra push" is required. Energetically, it is much more efficient to adsorb the linear *n*-butane to obtain higher loadings. For mixture adsorption, we note that total mixture loadings greater than four molecules per unit cell can be achieved only by adsorption of the linear nC4 (see Fig. 14c) [63, 64]. The MFI membrane permeation selectivity is found to be strongly in favour of the linear isomer [65, 66].

Another strategy is to exploit differences in the molecular footprints of the individual components [8]. To demonstrate this principle, let us consider the stacking of *cis*-2-butene and 1-butene within 1D channels of 6 Å (see Fig. 15). The footprint of *cis*-2-butene is smaller than that of 1-butene, so eight molecules of *cis*-2-butene can be packed within the chosen channel length. Only six molecules of 1-butene can locate within the same channel length. The differences in the packing efficiencies could be exploited to selectively adsorb *cis*-2-butene [8]. Tijsebaert et al. [67] have demonstrated the potential of RUB-41 all-silica zeolite, for this separation. RUB-41 comprises a two-dimensional intersecting channel system consisting of an eight-membered ring channel (2.7 × 5 Å) along [001], and a 10-membered ring channel (4 × 6.5 Å) along [100]. The measured data on adsorption indicates that the adsorption equilibrium follows the hierarchy of saturation capacities *cis*-2-butene > *trans*-2-butene >> 1-butene. Although this is not suggested by Tijsebaert, we believe that molecular length entropy effects provide the rationale for the observed hierarchy of adsorption [7, 8, 68, 69].
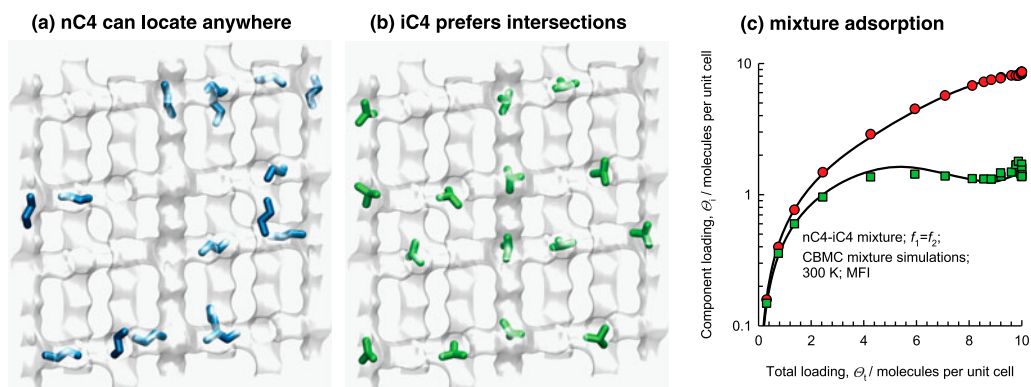

(a) nC4 can locate anywhere   **(b) iC4 prefers intersections**   **(c) mixture adsorption**

Fig. 14. Snapshots showing the location of (a) *n*-butane and (b) *iso*-butane within the intersecting channels of MFI zeolite. (c) Component loadings of *n*-butane and *iso*-butane for mixture adsorption.
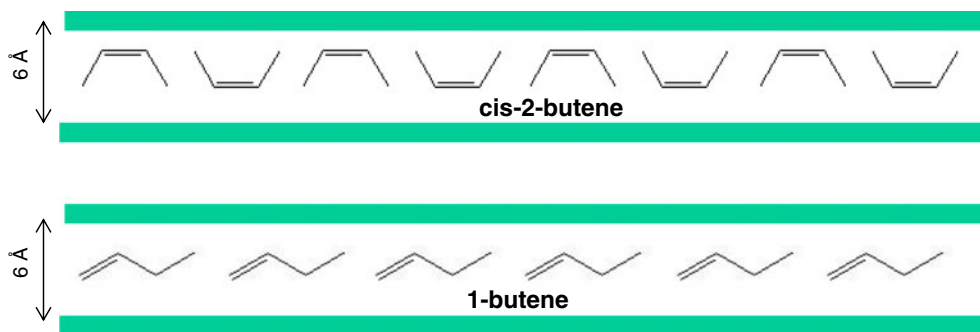
Fig. 15. Stacking of *cis*-2-butene (top row) and 1-butene (bottom row) within 1D channels of 6 Å.

Peng et al. [70] discuss the need for separation of CFC-115 (1-chloro-1,1,2,2,2-pentafluoroethane) and HFC-125 (1,1,1,2,2-pentafluoroethane). The boiling points of CFC-115 (234.1 K) and HFC-125 (224.7 K) are very close, and their mixtures can be nearly azeotropic. Therefore, cryogenic extractive distillation has been the dominant technology utilized to separate these mixtures. Adsorptive separations offer energy-efficient alternatives to distillation. Peng et al. [70] have reported the pure component isotherm data for CFC-115 and HFC-125 in MFI zeolite. CFC-115 locates preferentially at the intersections of MFI, because of the bulky Cl atom attached at the 1-position of CFC-115; as a consequence, the pure component isotherm shows an inflection at a loading of four molecules per unit cell. For total mixture loadings less than four molecules per unit cell, the adsorption selectivity is in favour of CFC-115. For mixture loadings greather than four molecules per unit cell, configurational entropy effects cause the adsorption selectivity to be in favour of HFC-125 [8].

Exploiting Packing Effects for Separation of Linear Alcohols

A different class of entropy effects manifests in adsorption of mixtures linear alcohols in cage-type zeolites, MOFs and ZIFs [8, 71, 72]. As illustration, Fig. 16(a, b) presents snapshots of the ethanol and 1-propanol adsorbed within the cages of CHA at saturation conditions. The cage diameter is 8.5 Å, and the size of the windows are approximately 3.8 Å. Since the cage capacity is limited, only a finite number of molecules can be packed within each cage; this number has to have an integer value. The saturation capacity of the ethanol is four molecules per cage; the saturation capacity of 1-propanol is smaller, two molecules per cage. The packing efficiency of ethanol is significantly higher than that of 1-propanol. For adsorption of ethanol/1-propanol for bulk phase conditions corresponding to saturation of the pores, packing entropy effects are significantly more favourable for the shorter alcohol. At total mixtures loadings less than molecules per cage, the adsorption selectivity is in favour the longer alcohol and has values in the range of 2–12 (Fig. 16c); this is "normal" behaviour. As the total mixture loadings increase to values higher than two molecules per cage, the adsorption selectivity is lower than unity, that is, in favour of the shorter alcohol. The reversal of selectivity is primarily due to the fact that it is not possible to achieve loadings greater than
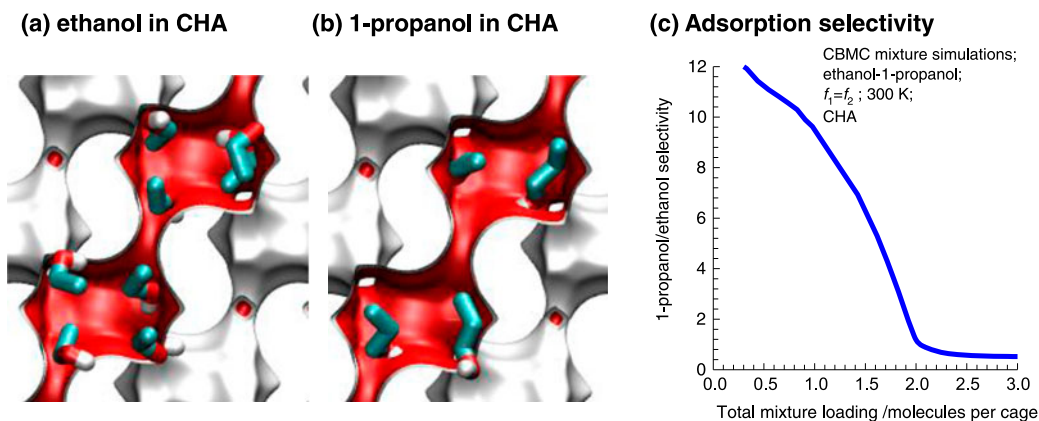
(a) ethanol in CHA   **(b) 1-propanol in CHA**   **(c) Adsorption selectivity**

Fig. 16. Snapshots showing the location and conformations of (a) ethanol, and (b) 1-propanol within the cages of CHA zeolite. (c) Adsorption selectivity of 1-propanol with respect to ethanol.

two molecules per cage for 1-propanol. The adsorbed phase contains predominantly the shorter alcohol owing to entropy effects [71]; this entropy-based separation is counter-intuitive because one should normally expect the longer alcohols to adsorb more strongly. This principle is confirmed by breakthrough experiments that were run under conditions close to saturation conditions within the cages [8, 73]. The same principle can be applied for selective adsorption of mixtures of linear alkanes with C numbers in excess of 30 using TSC zeolite; such separations have potential in lube oil refining [71].

Separating Xylene Isomers on the Basis of Stacking Efficiencies

The separation of C8 hydrocarbons is of great importance in the petrochemical industries. *Para*-xylene, the most valuable of the isomers, is primarily used as a feedstock (with purity requirement of 99%+) for terephthalic acid or dimethyl terephthalate, whose end uses include polyester fibers and polyethylene terephthalate resins for beverage bottles. The separation of C8 hydrocarbons by distillation is difficult because of the small differences in the boiling points (Fig. 17). There are, however, significant differences in the freezing points that allow fractional crystallization to be used for separations. The differences in the freezing points arise because of differences in the stacking efficiencies of molecules. *Para*-xylene has the highest freezing point because these molecules stack most efficiently; pure *p*-xylene crystals are the first to emerge from the solution upon cooling. However, the energy requirements for fractional crystallization are high because of the need to cool to temperatures of about 220 K.

Selective adsorption of xylene isomers within the pores of ordered crystalline micro-porous materials is an energy-efficient alternative to fractional crystallization. In principle, it is possible to separate *p*-xylene from this mixture if *p*-xylene is either the most strongly or the most weakly adsorbed component. Because of the *p*-xylene content of the feed is only about 20–25%, it is often easier to reach a high productivity with *p*-xylene-selective adsorbents [8, 74].
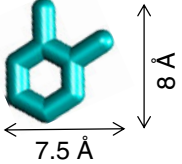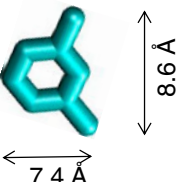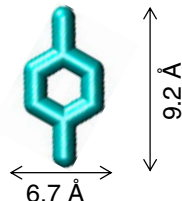
	Boiling point / K	Freezing point / K
o-xylene (oX)	417.6	248
m-xylene (mX)	412.3	222.5
p-xylene (pX)	411.5	286.4
n-octane (nC8)	398.8	216.4
Ethylbenzene(EtBz)	409.3	178.2
Styrene (St)	418.3	242.5

o-xylene dimensions: 8 Å × 7.5 Å
m-xylene dimensions: 8.6 Å × 7.4 Å
p-xylene dimensions: 9.2 Å × 6.7 Å

Fig. 17. Boiling points and freezing points of C8 hydrocarbons. The molecular dimensions of xylene isomers are taken from Peralta [74].

Let us see how we can proceed with the separation of C8 hydrocarbons. Ethylbenzene is not a flat molecule; the ethyl branch is not in the same plane as the benzene ring. The xylene isomers are flat; these isomers can align themselves parallel to the channel walls, affording better van der Waals interactions with the framework atoms. Depending on the choice of the channel dimensions, the efficiencies with which the xylene isomers pack within the channels are different because of the differences in the molecular dimensions of the xylene isomers. The height and width of the xylene isomers are: *o*-xylene, 8 × 7.5 Å; *m*-xylene, 8.6 × 7.4 Å; *p*-xylene, 9.2 × 6.7 Å; see dimensions provided in Fig. 17.

Consider the stacking of *o*-xylene and *p*-xylene within 1D channels that are about 8.5 Å wide (see Fig. 18). With this choice of channel dimension, the stacking efficiency of *o*-xylene is higher than that of *p*-xylene; that is, more *o*-xylene molecules can be packed within a
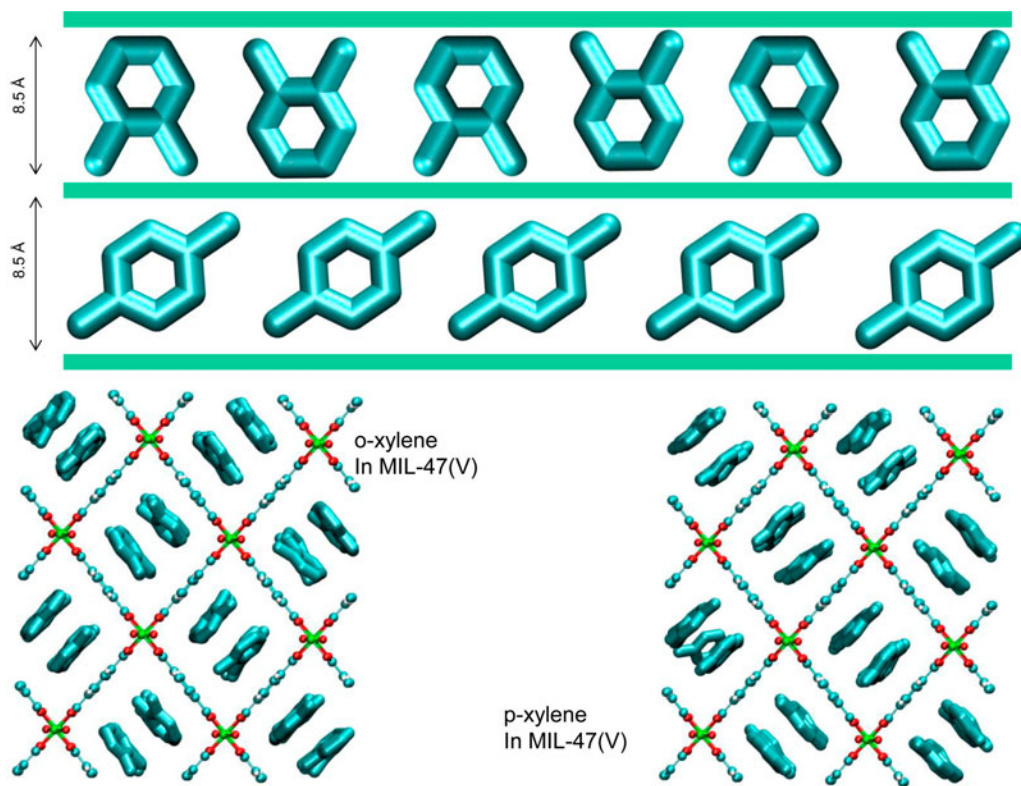
Fig. 18. Stacking of o-xylene and p-xylene within the 1D 8.5 Å channels. The head-on snapshots of *o*-xylene and *p*-xylene adsorbed within the channels of MIL-47(V) are shown in the bottom row.

channel of a given length. The channel size is not wide-enough to allow *p*-xylene to stack vertically, and fewer molecules can be packed within the same channel length. Experimental data [75, 76] for MIL-47(V) and MIL-53(Al) with 1D rhombohedric channels of 8.5 Å confirm that these MOFs are selective to adsorption of the *o*-xylene [8] when operating at conditions close to saturation of the channels.

If the 1D channels are wider, say about 10 Å, then *p*-xylene isomers can stack vertically (Fig. 19). Molecular simulations for adsorption of xylene isomers in Co(BDP), which has 10 Å 1D channels, confirm that this MOF is *para* selective [7, 8]. Stacking xylenes within 1D channels is analogous to stacking books within bookshelves [8].

The separation of ethylbenzene and styrene is necessary in the production of polystyrene [8]. The differences in the boiling points is just 9 K, necessitating the use of sub-atmospheric pressure operations, which is energy demanding. Adsorptive separation of ethylbenzene/ styrene mixtures can be realized by exploiting the differences in the degrees of flatness of ethylbenzene and styrene, coupled with the interactions with the framework atoms of MIL-47 (V) and MIL-53 (Al) [77, 78]. Both these MOFs are selective to adsorption of styrene.
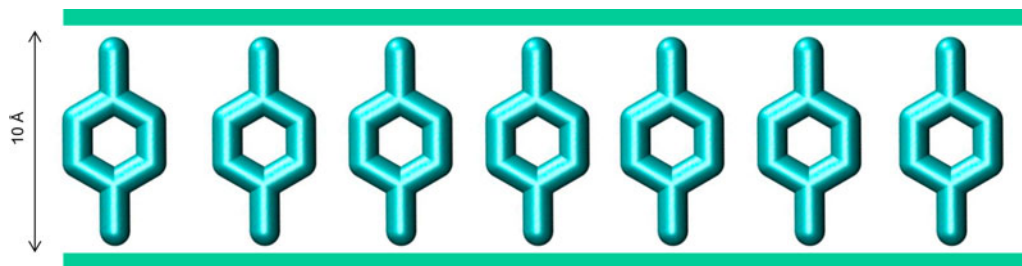
Fig. 19. Stacking of *p*-xylene within the 1D 10 Å channels.

A *Pot Pourri* of Strategies for Separating Hexane Isomers

The separation of hexane isomers, *n*-hexane (nC6), 2-methylpentane (2MP), 3-methylpentane (3MP), 2,2-dimethylbutane (22DMB) and 2,3 dimethylbutane (23DMB) is required for production of high-octane gasoline; the di-branched isomers have the highest research octane number (RON) rating and are the preferred components for incorporation into the gasoline pool [8, 18, 79]. Currently, the separation of the products from the isomerization reactor is performed using LTA-5A zeolite that operates on the principle of molecular sieving. Linear nC6 can hop from one cage to the adjacent cage through the 4 Å windows, but branched alkanes are largely excluded. We need a separation device that would separate the di-branched isomers 22DMB and 23DMB from the nC6, 2MP and 3MP. Such a separation is not feasible with the currently used LTA-5A.

Herm et al. [80] report the synthesis of a bespoke-tailored material $Fe_2(BDP)_3$ [BDP^{2-} = benzenedipyrazolate] that has 1D channels which are triangular in shape and a pore size of 4.9 Å (see Fig. 20). Molecular simulations provide insights into the workings of $Fe_2(BDP)_3$.
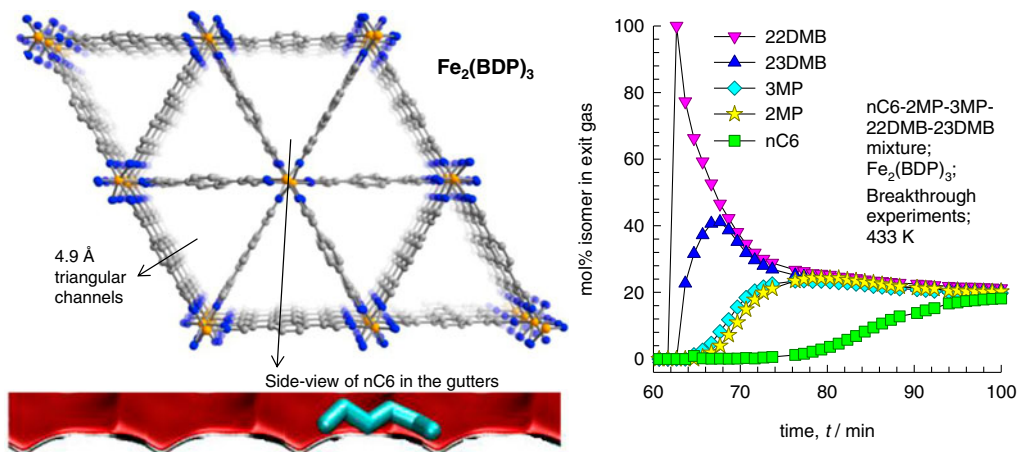

Fig. 20. (a) The triangular framework of $Fe_2(BDP)_3$. (b) Transient breakthrough of hexane isomers in a fixed bed packed with $Fe_2(BDP)_3$.

The linear nC6 can align optimally along the V-shaped gutters, and exert the best van der Waals interaction with the framework. The interactions of the mono- and di-branched isomers are less effective, resulting in considerably lower adsorption strengths. The hierarchy of breakthroughs reported in the transient experiments of Herm et al. [80] is 22DMB, 23DMB, 3MP, 2MP and nC6; this hierarchy is dictated by a combination of adsorption strengths (nC6 > > 2MP ≈ 3MP >> 22DMB ≈ 23DMB) and diffusivities (nC6 > 2MP ≈ 3MP > 22DMB ≈ 23DMB). The di-branched isomers 22DMB and 23DMB can be recovered in the early stages of the breakthrough; this is the desired high RON product.

CFI and ATS zeolites, patented by Chevron for application in the alkane isomerization process [81, 82], have 1D channels similar to that of AFI zeolite [8, 80]. The hierarchy of adsorption strengths is nC6 < (2MP, 3MP) << (22DMB, 23DMB); this is primarily dictated by the molecular footprints (see Fig. 21). The linear nC6 has a longer "footprint" and occupies a larger segment of the channel. 22DMB and 23DMB are the most compact molecules and have the smallest footprint; consequently, more di-branched isomers can be located within a given length of the channels when compared with nC6. 2MP and 3MP have footprints that have an intermediate character. Molecular length entropy effects dictates the sorption hierarchy in CFI and ATS; a similar situation holds for MOR that has 6.5 × 7 Å sized 1D channels [7, 8, 68, 69].

The "fractionation" of hexane isomers into three different fractions is achieved with MFI zeolite in a completely different manner by exploiting subtle configurational differences [8, 18, 83], discussed earlier for nC4/iC4 mixtures. The linear nC6 can locate comfortably along the channels (see Fig. 22a). The mono-branched and di-branched isomers locate preferentially at the channel intersections that offer more "leg-room" for these bulkier, more-compact, branched isomers. However, the number of intersections is limited to four per unit cell; this limits the saturation capacities. Figure 22(b) presents configurational-bias Monte Carlo simulations of component loadings in a five-component nC6/2MP/3MP/22DMB/23DMB mixture as the total mixture loading Θ_t. Configurational entropy effects manifest at $\Theta_t > 4$, causing the hierarchy of component loadings to be nC6 > 2MP > 3MP > 23DMB > 22DMB. The configurational-entropy principle to separate hexane isomers using MFI zeolite was first elucidated using configurational-bias Monte Carlo simulations [8, 83–85]. The di-branched isomers have significantly lower diffusivities, and the separations in fixed bed adsorbers benefit from the synergy between adsorption and diffusion [8]. The transient breakthrough of hexane isomers in a fixed bed adsorber packed with MFI zeolite shows the sequence 22DMB,
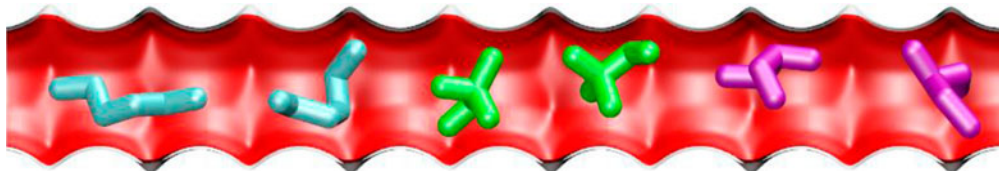

Fig. 21. Differences in molecular footprints of nC6, 3MP, and 22DMB within 1D 7.3 Å channels of AFI zeolite.

(a) Snapshot of hexane isomers
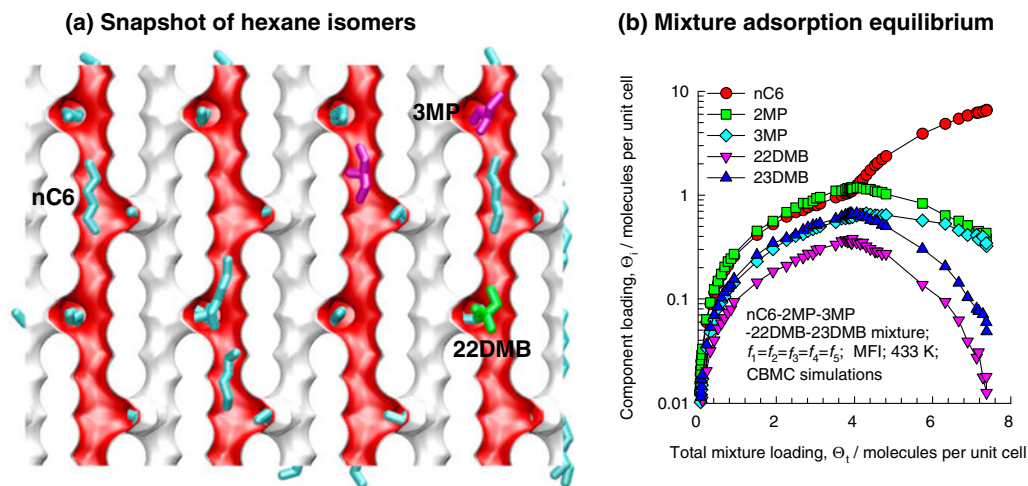
(b) Mixture adsorption equilibrium

Fig. 22. (a) Snapshots showing the location of nC6, 3MP and 22DMB within the MFI zeolite. (b) configurational-bias Monte Carlo simulations of the component loadings of hexane isomers as a function of the total mixture loading.

23DMB, 3MP, 2MP, nC6. The desired high RON products 22DMB and 23DMB can be recovered in the early stages of the breakthrough; this satisfies the process requirements.

Distinguishing *Rectus* and *Sinister* Configurations

Many natural and synthetic compounds are chiral, which means they can exist in right- (*R*- = *rectus*) or left- (*S*- = *sinister*) handed forms that are mirror images of each other. Often, only one of these forms is biologically active as drugs. Vaidhyanathan et al. [86] report separations of nine different chiral diols using the homochiral Ni_2(L-asp)$_2$(bipy) formed by Ni (L-aspartic
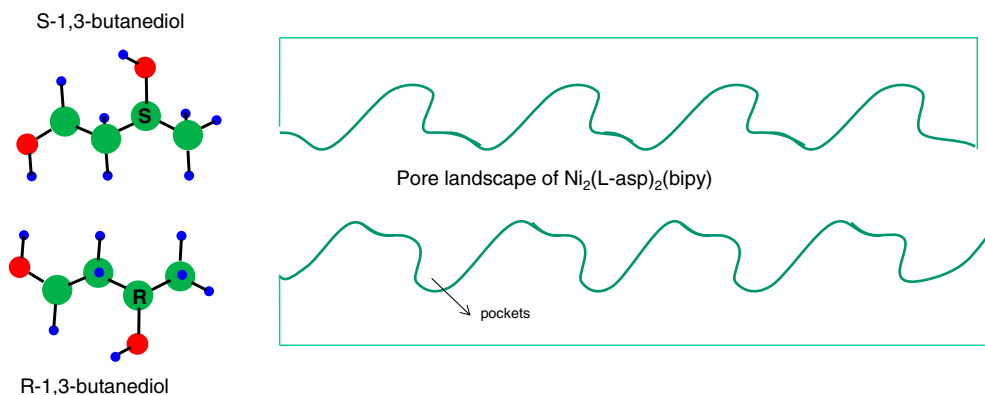

Fig. 23. Separation of *R*-1,3-butanediol and *S*-1,3-butanediol using homochiral metal-organic framework Ni_2(L-asp)$_2$(bipy).

acid) clusters connected by 4,4′-bipyridine ligands. For separation of 1,3-butanediol, the value of the enantiomeric excess, *ee*, is 18%. The mechanism for adsorption of either *R*- or *S*-forms is rationalized on the basis of molecular simulations. The pore landscape, sketched in Fig. 23], using data from molecular simulations [87], shows the existence of pockets within the 3.5 Å sized pores. The preference for the *R*- form is due to the more effective occupation of the pore space and pockets of $Ni_2(L\text{-asp})_2(bipy)$.

Huang et al. [88] fabricated an $Ni_2(L\text{-asp})_2(bipy)$ membrane and demonstrated the feasibility of separating racaemic 2-methyl-2,4-pentanediol to obtain a permeate with *ee* =35%. Das et al. [89] showed that mixed-metal organic frameworks have the ability to separate chiral alcohols 1-phenylethanol, 2-butanol and 2-pentanol with *ee* values ranging to 82%.

Conclusions

In this paper we have offered a smörgåsbord of separation strategies that are offered by use of ordered microporous crystalline materials. In addition to exploiting differences in binding energies of the components (based on van der Waals interactions, electrostatic interactions, π-electron exchanges), we may exploit the inter-play between adsorption and diffusion. Subtle differences in molecular configurations and molecular conformations offer entropy-based mixture separation possibilities. Differences in the efficiencies of packing or stacking of molecules can be exploited to achieve separations that favour the molecules that can be packed most efficiently. Differences in packing efficiencies are the key for separation of xylene isomers.

References

1. "Materials for Separation Technologies: Energy and Emission Reduction Opportunities", US Department of Energy, Energy Efficiency and Renewable Energy, 2005, https://www1.eere.energy.gov/manufacturing/industries_technologies/imf/pdfs/separationsreport.pdf

2. Férey, G., "Hybrid Porous Solids: Past, Present, Future", *Chem Soc Rev.*, **37**, pp. 191–214 (2008).

3. Furukawa, H., Cordova, K.E., O'Keeffe, M. and Yaghi, O.M., "The Chemistry and Applications of Metal–Organic Frameworks", *Science*, **341**, pp. 2040–2042 (2013).

4. Banerjee, R., Phan, A., Wang, B., Knobler, C., Furukawa, H., O'Keeffe, M. and Yaghi, O.M., "High-throughput Synthesis of Zeolitic Imidazolate Frameworks and Application to CO_2 Capture", *Science*, **319**, pp. 939–943 (2008).

5. Yaghi, O.M., O'Keeffe, M., Ockwig, N.W., Chae, H.K., Eddaoudi, M. and Kim, J. "Reticular Synthesis and the Design of New Materials", *Nature*, **423**, pp. 705–714 (2003).

6. Krishna, R. and van Baten, J.M., "In Silico Screening of Zeolite Membranes for CO_2 Capture", *J Membr Sci*, **360**, pp. 323–333 (2010).

7. Krishna, R. and van Baten, J.M., "In Silico Screening of Metal–Organic Frameworks in Separation Applications", *Phys Chem Chem Phys.*, **13**, pp. 10593–10616 (2011).

8. Krishna, R., "The Maxwell–Stefan Description of Mixture Diffusion in Nanoporous Crystalline Materials", *Microporous Mesoporous Mater.*, **185**, pp. 30–50 (2014).

9. Krishna, R., "Diffusion in Porous Crystalline Materials", *Chem Soc Rev*, **41**, pp. 3099–3118 (2012).

10. Krishna, R., "Describing the Diffusion of Guest Molecules inside Porous Structures", *J Phys Chem C*, **113**, pp. 19756–19781 (2009).

11. Krishna, R. and van Baten, J.M., "Investigating the Relative Influences of Molecular Dimensions and Binding Energies on Diffusivities of Guest Species Inside Nanoporous Crystalline Materials", *J Phys Chem C*, **116**, pp. 23556–23568 (2012).

12. Krishna, R. and van Baten, J.M., "A Molecular Dynamics Investigation of the Diffusion Characteristics of Cavity-type Zeolites with 8-Ring Windows", *Microporous Mesoporous Mater*, **137**, pp. 83–91 (2011).

13. Lee, Y., Hriljac, J.A., Vogt, T., Parise, J.B., Edmondson, M.J., Anderson, P.A., Corbin, D.R. and Nagai, T., "Phase Transition of Zeolite RHO at High-Pressure", *J Am Chem Soc*, **123**, pp. 8418–8419 (2001).

14. Dubbeldam, D., Walton, K.S., Ellis, D.E. and Snurr, R.Q., "Exceptional Negative Thermal Expansion in Isoreticular Metal–Organic Frameworks", *Angew Chem Int Ed*, **46**, pp. 4496–4499 (2007).

15. Serre, C., Millange, F., Thouvenot, C., Nouguès, M., Marsolier, G., Louër, D. and Férey, G., "Very Large Breathing Effect in the First Nanoporous Chromium(III)-based Solids: MIL-53 or $Cr^{III}(OH).\{O_2C–C_6H_4–CO_2\}.\{HO_2C–C_6H_4–CO_2H\}_x.H_2O_{y/'}$", *J Am Chem Soc*, **124**, pp. 13519–13526 (2002).

16. Dubbeldam, D., Krishna, R. and Snurr, R.Q., "Method for Analyzing the Alterations in the Crystal Structures of Metal–Organic Frameworks", *J Phys Chem C*, **113**, pp. 19317–19327 (2009).

17. Horcajada, P., Serre, C., Maurin, G., Ramsahye, N.A., Balas, F., Vallet-Regí, M., Sebban, M., Taulelle, F. and Férey, G., "Flexible Porous Metal–Organic Frameworks for a Controlled Drug Delivery *J Am Chem Soc*, **130**, pp. 6774–6780 (2008).

18. Krishna, R. and van Baten, J.M., "Screening of Zeolite Adsorbents for Separation of Hexane Isomers: A Molecular Simulation Study", *Sep Purif Technol*, **55**, pp. 246–255 (2007).

19. Krishna, R. and van Baten, J.M., "Using Molecular Simulations for Screening of Zeolites for Separation of CO_2/CH_4 Mixtures", *Chem Eng J*, **133**, pp. 121–131 (2007).

20. Krishna, R. and van Baten, J.M., "A Comparison of the CO_2 Capture Characteristics of Zeolites and Metal–Organic Frameworks", *Sep Purif Technol*, **87**, pp. 120–126 (2012).

21. Wu, H., Yao, K., Zhu, Y., Li, B., Shi, Z., Krishna, R. and Li, J., "Cu-TDPAT, an *rht*-type Dual-Functional Metal–Organic Framework Offering Significant Potential for Use in H_2 and Natural Gas Purification Processes Operating at High Pressures *J Phys Chem C*, **116**, pp. 16609–16618 (2012).

22. Xiang, S.C., He, Y., Zhang, Z., Wu, H., Zhou, W., Krishna, R. and Chen, B., "Microporous Metal–Organic Framework with Potential for Carbon Dioxide Capture at Ambient Conditions", *Nat Commun*, **3**, p. 954 (2012), http://dx.doi.org/doi:10.1038/ncomms1956

23. Herm, Z.R., Krishna, R. and Long, J.R., "CO_2/CH_4, CH_4/H_2 and $CO_2/CH_4/H_2$ separations at high pressures using Mg_2(dobdc)", *Microporous Mesoporous Mater*, **151**, pp. 481–487 (2012).

24. Herm, Z.R., Swisher, J.A., Smit, B., Krishna, R. and Long, J.R., "Metal–Organic Frameworks as Adsorbents for Hydrogen Purification and Pre–Combustion Carbon Dioxide Capture", *J Am Chem Soc*, **133**, pp. 5664–5667 (2011).

25. Mason, J.A., Sumida, K., Herm, Z.R., Krishna, R. and Long, J.R., "Evaluating Metal–Organic Frameworks for Post-Combustion Carbon Dioxide Capture via Temperature Swing Adsorption", *Energy Environ Sci*, **4**, pp. 3030–3040 (2011).

26. McDonald, T.M., D'Alessandro, D.M., Krishna, R. and Long, J.R., "Enhanced Carbon Dioxide Capture upon Incorporation of *N,N′*-Dimethylethylenediamine in the Metal–Organic Framework CuBTTri", *Chem Sci*, **2**, pp. 2022–2028 (2011).

27. Yang, J., Krishna, R., Li, J. and Li, J., "Experiments and Simulations on Separating a CO_2/CH_4 Mixture using K-KFI at Low and High Pressures", *Microporous Mesoporous Mater*, **184**, pp. 21–27 (2014).

28. "Basic Research Needs for Carbon Capture: Beyond 2020", US Department of Energy, Office of Science, Basic Energy Sciences, 2010, http://www.science.doe.gov/bes/reports/abstracts.html#CC B2020

29. Duan, J., Higuchi, M., Krishna, R., Kiyonaga, T., Tsutsumi, Y., Sato, Y., Kubota, Y., Takata, M. and Kitagawa, S., "High $CO_2/N_2/O_2/CO$ Separation in a Chemically Robust Porous Coordination Polymer with Low Binding Energy", *Chem Sci*, **5**, pp. 660–666 (2014).

30. Krishna, R., "Adsorptive Separation of $CO_2/CH_4/CO$ Gas Mixtures at High Pressures", *Microporous Mesoporous Mater*, **156**, pp. 217–223 (2012).

31. Chavan, S., Bonino, F., Valenzano, L., Civalleri, B., Lamberti, C., Acerbi, N., Cavka, J.H., Leistner, M. and Bordiga, S., "Fundamental Aspects of H_2S Adsorption on CPO-27-Ni", *J Phys Chem C*, **117**, pp. 15615–15622 (2013).

32. Vaesen, S., Guillerm, V., Yang, Q., Wiersum, A.D., Marszalek, B., Gil, B., Vimont, A., Daturi, M., Devic, T., Llewellyn, P.L., Serre, C., Maurin, G. and De Weireld, G., "A Robust Amino-functionalized Titanium(IV) Based MOF for Improved Separation of Acid Gases", *Chem Commun*, **49**, pp. 10082–10084 (2013).

33. Britt, D., Tranchemontagne, D. and Yaghi, O.M., "Metal–Organic Frameworks with High Capacity and Selectivity for Harmful Gases", *Proc Natl Acad Sci USA*,. **105**, pp. 11623–11627 (2008).

34. He, Y., Krishna, R. and Chen, B., "Metal–Organic Frameworks with Potential for Energy-Efficient Adsorptive Separation of Light Hydrocarbons", *Energy Environ Sci*, **5**, pp. 9107–9120 (2012).

35. Bloch, E.D., Queen, W.L., Krishna, R., Zadrozny, J.M., Brown, C.M. and Long, J.R., "Hydrocarbon Separations in a Metal–Organic Framework with Open Iron(II) Coordination Sites", *Science*, **335**, pp. 1606–1610 (2012).

36. Chavan, S.M., Shearer, G.C., Bloch, E.D. and Bordiga, S., "Acetylene Adsorption on CPO-27-M Metal–Organic Frameworks (M = Fe, Co and Ni)", *Chem Phys Chem*, **13**, pp. 445–448 (2012).

37. Gücüyener, C., van den Bergh, J., Gascon, J. and Kapteijn, F., "Ethane/Ethene Separation Turned on Its Head: Selective Ethane Adsorption on the Metal–Organic Framework ZIF-7 through a Gate-Opening Mechanism", *J Am Chem Soc*, **132**, pp. 17704–17706 (2010).

38. Kim, J., Lin, L.-C., Martin, R.L., Swisher, J.A., Haranczyk, M. and Smit, B., "Large-Scale Computational Screening of Zeolites for Ethane/Ethene Separation", *Langmuir*, **28**, pp. 11914–11919 (2012).

39. Böhme, U., Barth, B., Paula, C., Kuhnt, A., Schwieger, W., Alexander Mundstock, A., Caro, J. and Hartmann, M., "Ethene/Ethane and Propene/Propane Separation via the Olefin and Paraffin Selective Metal Organic Framework Adsorbents CPO-27 and ZIF8", *Langmuir*, **29**, pp. 8592–8600 (2013).

40. He, Y., Xiong, S., Zhang, Z., Xiong, S., Fronczek, F.R., Krishna, R., O'Keeffe, M. and Chen, B., "A Microporous Lanthanide–Tricarboxylate Framework with the Potential for Purification of Natural Gas", *Chem Commun*, **48**, pp. 10856–10858 (2012).

41. Tavan, Y., Shahhosseini, S. and Hosseini, S.H., "Feed-splitting Technique in the Extractive Distillation of CO$_2$-Ethane Azeotropic Process", *Sep Purif Technol* **122**, pp. 47–53 (2014).

42. Liu, J., Thallapally, P.K. and Strachan, D., "Metal Organic Frameworks for Removal of Xe and Kr from Nuclear Fuel Reprocessing Plants", *Langmuir*, **28**, pp. 11584–11589 (2012).

43. Takahashi, A. and Yang, R.T., "New Adsorbents for Purification: Selective Removal of Aromatics", *AIChEJ*, **48**, pp. 1457–1468 (2002).

44. Ren, H., Ben, T., Wang, E., Jing, X., Xue, M., Liu, B., Cui, Y., Qui, S. and Zhu, G., "Targeted Synthesis of a 3D Porous Aromatic Framework for Selective Sorption of Benzene", *Chem Commun*, **46**, pp. 291–293 (2010).

45. Krishna, R., Goswami, A.N., Nanoti, S.M., Rawat, B.S., Khanna, M.K. and Dobhal, J., "Extraction of Aromatics from 63–69 °C Naphtha Fraction for Food Grade Hexane Production Using Sulpholane and NMP as Solvents", *Indian J Technol*, **25**, pp. 602–606 (1987).

46. Pluth, J.J. and Smith, J.V., "Accurate Redetermination of Crystal Structure of Dehydrated Zeolite A. Absence of Near Zero Coordination of Sodium. Refinement of Silicon, Aluminum-ordered Superstructure", *J Am Chem Soc*, **102**, pp. 4704–4708 (1980).

47. García-Sánchez, A., García-Pérez, E., Dubbeldam, D., Krishna, R. and Calero, S., "A Simulation Study of Alkanes in Linde Type A Zeolites", *Adsorpt Sci Technol*, **25**, pp. 417–427 (2007).

48. Hedin, N., DeMartin, G.J., Roth, W.J., Strohmaier, K.G. and Reyes, S.C., "PFG NMR self-diffusion of small hydrocarbons in high silica DDR, CHA and LTA structures", *Microporous Mesoporous Mater*, **109**, pp. 327–334 (2008).

49. Hedin, N., DeMartin, G.J., Strohmaier, K.G. and Reyes, S.C., "PFG NMR self-diffusion of propylene in ITQ-29, CaA and NaCaA: Window size and cation effects", *Microporous Mesoporous Mater*, **98**, pp. 182–188 (2007).

50. Fritzsche, S., Haberlandt, R., Kärger, J., Pfeifer, H., Heinzinger, K. and Wolfsberg, M., "Influence of Exchangeable Cations on the Diffusion of Neutral Diffusants in Zeolites of Type LTA – an MD Study", *Chem Phys Lett*, **242**, pp. 361–366 (1995).

51. Simo, M., Sivashanmugam, S., Brown, C.J. and Hlavacek, V., "Adsorption/Desorption of Water and Ethanol on 3A Zeolite in Near-Adiabatic Fixed Bed", *Ind Eng Chem Res.*, **48**, pp. 9257–9260 (2009).

52. Krishna, R. and van Baten, J.M., "Influence of Adsorption Thermodynamics on Guest Diffusivities in Nanoporous Crystalline Materials", *Phys Chem Chem Phys*, **15**, pp. 7994–8016 (2013).

53. Colon, Y.J., Krishna, R. and Snurr, R.Q., "Strong Influence of the H$_2$ Binding Energy on the Maxwell–Stefan Diffusivity in NU-100, UiO-68, and IRMOF-16", *Microporous Mesoporous Mater* **185**, pp. 190–196 (2014).

54. Bloch, E.D., Murray, L., Queen, W.L., Chavan, S.M., Maximoff, S.N., Bigi, J.P., Krishna, R., Peterson, V.K., Grandjean, F., Long, G.J., Smit, B., Bordiga, S., Brown, C.M. and Long, J.R., "Selective Binding of O$_2$ over N$_2$ in a Redox-Active Metal–Organic Framework with Open Iron(II) Coordination Sites", *J Am Chem Soc*, **133**, pp. 14814–14822 (2011).

55. Zhang, K., Lively, R.P., Zhang, C., Koros, W.J. and Chance, R.R., "Investigating the Intrinsic Ethanol/Water Separation Capability of ZIF-8: An Adsorption and Diffusion Study", *J Phys Chem C*, **117**, pp. 7214–7225 (2013).

56. Zhang, K., Lively, R.P., Zhang, C., Chance, R.R., Koros, W.J., Sholl, D.S. and Nair, S., "Exploring the Framework Hydrophobicity and Flexibility of ZIF-8: From Biofuel Recovery

to Hydrocarbon Separations", *J Phys Chem Lett*., **4**, pp. 3618–3622 (2013). doi:10.1021/jz 402019d

57. Bhadra, S.J. and Farooq, S., "Separation of Methane–Nitrogen Mixture by Pressure Swing Adsorption for Natural Gas Upgrading", *Ind Eng Chem Res*, **50**, pp. 14030–14045 (2011).

58. Majumdar, B., Bhadra, S.J., Marathe, R.P. and Farooq, S., "Adsorption and Diffusion of Methane and Nitrogen in Barium Exchanged ETS-4", *Ind Eng Chem Res*, **50**, pp. 3021–3034 (2011).

59. Kuznicki, S.M., Bell, V.A., Nair, S., Hillhouse, H.W., Jacubinas, R.M., Braunbarth, C.M., Toby, B.H. and Tsapatsis, M., "A Titanosilicate Molecular Sieve with Adjustable Pores for Size-selective Adsorption of Molecules", *Nature*, **412**, pp. 720–724 (2001).

60. Liu, D., Ma, X., Xi, H. and Lin, Y.S., "Gas Transport Properties and Propylene/propane Separation Characteristics of ZIF-8 Membranes", *J Membr Sci*., **451**, pp. 85–93 (2014).

61. Pan, Y., Li, T., Lestari, G. and Lai, Z., "Effective Separation of Propylene/Propane Binary Mixtures by ZIF-8 Membranes", *J Membr Sci*, **390–391**, pp. 93–98 (2012).

62. Hartmann, M., Kunz, S., Himsl, D., Tangermann, O., Ernst, S. and Wagener, A., "Adsorptive Separation of Isobutene and Isobutane on $Cu_3(BTC)_2$", *Langmuir*, **24**, pp. 8634–8642 (2008).

63. Krishna, R. and Paschek, D., "Separation of Hydrocarbon Mixtures using Zeolite Membranes: A Modelling Approach Combining Molecular Simulations with the Maxwell–Stefan Theory", *Sep Purif Technol*, **21**, pp. 111–136 (2000).

64. Krishna, R. and Paschek, D., "Molecular Simulations of Adsorption and Siting of Light Alkanes in Silicalite-1", *Phys Chem Chem Phys*, **3**, pp. 453–462 (2001).

65. Matsufuji, T., Nishiyama, N., Matsukata, M. and Ueyama, K., "Separation of Butane and Xylene Isomers with MFI-type Zeolitic Membrane Synthesized by a Vapor-phase Transport Method", *J Membr Sci*, **178**, pp. 25–34 (2000).

66. Vroon, Z.A.E.P., Keizer, K., Gilde, M.J., Verweij, H. and Burggraaf, A.J., "Transport Properties of Alkanes Through Ceramic Thin Zeolife MFI Membranes", *J Membr Sci*, **113**, pp. 293–300 (1996).

67. Tijsebaert, B., Varszegi, C., Gies, H., Xiao, F.S., Bao, X., Tatsumi, T., Müller, U. and De Vos, D., "Liquid Phase Separation of 1-Butene from 2-Butenes on All-silica Zeolite RUB-41", *Chem Commun*., pp. 2480–2482 (2008).

68. Krishna, R., Smit, B. and Calero, S., "Entropy Effects During Sorption of Alkanes in Zeolites", *Chem Soc Rev*, **31**, pp. 185–194 (2002).

69. van Baten, J.M. and Krishna, R., "Entropy Effects in Adsorption and Diffusion of Alkane Isomers in Mordenite: An Investigation Using CBMC and MD Simulations", *Microporous Mesoporous Mater*, **84**, pp. 179–191 (2005).

70. Peng, Y., Zhang, Z., Zheng, X., Wang, H., Xu, C., Xiao, Q., Zhong, Y. and Zhu, W., "Comparison Study on the Adsorption of CFC-115 and HFC-125 on Activated Carbon and Silicalite-1", *Ind Eng Chem Res*, **49**, pp. 10009–10015 (2010).

71. Krishna, R. and van Baten, J.M., "Entropy-based Separation of Linear Chain Molecules by Exploiting Differences in the Saturation Capacities in Cage-type Zeolites", *Sep Purif Technol*, **76**, pp. 325–330 (2011).

72. Krishna, R. and van Baten, J.M., "Separating *n*-Alkane Mixtures by Exploiting Differences in the Adsorption Capacity within Cages of CHA, AFX and ERI zeolites", *Sep Purif Technol*, **60**, pp. 315–320 (2008).

73. Remy, T., Saint-Remi, J.C., Singh, R., Webley, P.A., Baron, G.V. and Denayer, J.F.M., "Adsorption and Separation of C1–C8 Alcohols on SAPO-34", *J Phys Chem C*, **115**, pp. 8117–8125 (2011).

74. Peralta, D., Barthelet, K., Pérez-Pellitero, J., Chizallet, C., Chaplais, G., Simon-Masseron, A. and Pirngruber, G.D., "Adsorption and Separation of Xylene Isomers: CPO-27-Ni vs HKUST-1 vs NaY", *J Phys Chem C*, **116**, pp. 21844–21855 (2012).

75. Finsy, V., Verelst, H., Alaerts, L., De Vos, D., Jacobs, P.A., Baron, G.V. and Denayer, J.F.M., "Pore-Filling-Dependent Selectivity Effects in the Vapor-Phase Separation of Xylene Isomers on the Metal–Organic Framework MIL-47", *J Am Chem Soc*, **130**, pp. 7110–7118 (2008).

76. Remy, T., Baron, G.V. and Denayer, J.F.M., "Modeling the Effect of Structural Changes during Dynamic Separation Processes on MOFs", *Langmuir*, **27**, pp. 13064–13071 (2011).

77. Maes, M., Vermoortele, F., Alaerts, L., Couck, S., Kirschhock, C.E.A., Denayer, J.F.M. and De Vos, D.E., "Separation of Styrene and Ethylbenzene on Metal–Organic Frameworks: Analogous Structures with Different Adsorption Mechanisms", *J Am Chem Soc*, **132**, pp. 15277–15285 (2010).

78. Remy, T., Ma, L., Maes, M., De Vos, D.E., Baron, G.V. and Denayer, J.F.M., "Vapor-phase Adsorption and Separation of Ethylbenzene and Styrene on the Metal Organic Frameworks MIL-47 and MIL-53(Al)", *Ind Eng Chem Res*, **51**, pp. 14824–14833 (2012).

79. Dubbeldam, D., Krishna, R., Calero, S. and Yazaydın, A.Ö., "Computer-assisted Screening of Ordered Crystalline Nanoporous Adsorbents for Separation of Alkane Isomers", *Angew Chem Int Ed*, **51**, pp. 11867–11871 (2012).

80. Herm, Z.R., Wiers, B.M., Van Baten, J.M., Hudson, M.R., Zajdel, P., Brown, C.M., Maschiocchi, N., Krishna, R. and Long, J.R., "Separation of Hexane Isomers in a Metal–Organic Framework with Triangular Channels", *Science*, **340**, pp. 960–964 (2013).

81. Maesen, T. and Harris, T., "Process for Producing High RON Gasoline Using CFI Zeolite", Chevron USA Inc., San RamonCA, US, US Patent, US 70374222 B2, 2006.

82. Maesen, T. and Harris, T., "Process for Producing High RON Gasoline Using ATS Zeolite", Chevron USA Inc., San RamonCA, US, US Patent, US 7029572 B2, 2006.

83. Krishna, R., "Exploiting Configurational Entropy Effects for Separation of Hexane Isomers using Silicalite-1", *Chem Eng Res Des*, **79**, pp. 182–194 (2001).

84. Krishna, R., Smit, B. and Vlugt, T.J.H., "Sorption-induced Diffusion-selective Separation of Hydrocarbon Isomers using Silicalite", *J Phys Chem A*, **102**, pp. 7727–7730 (1998).

85. Vlugt, T.J.H., Krishna, R. and Smit, B., "Molecular Simulations of Adsorption Isotherms for Linear and Branched Alkanes and Their Mixtures in Silicalite", *J Phys Chem B*, **103**, pp. 1102–1118 (1999).

86. Vaidhyanathan, R., Bradshaw, D., Rebilly, J.-N., Barrio, J.P., Gould, J.A., Berry, N.G. and Rosseinsky, M.J., "A Family of Nanoporous Materials Based on an Amino Acid Backbone", *Angew Chem Int Ed*, **45**, pp. 6495–6499 (2006).

87. Moghadam, P.Z. and Düren, T., "Origin of Enantioselectivity in a Chiral Metal Organic Framework: A Molecular Simulation Study", *J Phys Chem C*, **116**, pp. 20874–20881 (2012).

88. Huang, K., Dong, X., Ren, R. and Jin, W., "Fabrication of Homochiral Metal–Organic Framework Membrane for Enantioseparation of Racemic Diols", *AIChEJ*, **59**, pp. 4364–4372 (2013).

89. Das, M.C., Guo, Q., He, Y., Kim, J., Zhao, C.G., Hong, K., Xiang, S., Zhang, Z., Thomas, K.M., Krishna, R. and Chen, B., "Interplay of Metalloligand and Organic Ligand to Tune Micropores

within Isostructural Mixed-Metal Organic Frameworks (M'MOFs) for Their Highly Selective Separation of Chiral and Achiral Small Molecules", *J Am Chem Soc*, **134**, pp. 8703–8710 (2012).

90. Wu, H., Simmons, J.M., Srinivas, G., Zhou, W. and Yildrim, T., "Adsorption Sites and Binding Nature of CO_2 in Prototypical Metal–Organic Frameworks: A Combined Neutron Diffraction and First-Principles Study", *J Phys Chem Lett*, **1**, pp. 1946–1951 (2010).